The freeze-out mechanism and phase-space density in ultrarelativistic heavy-ion collisions

Boris Tomášik and Urs Achim Wiedemann
CERN, Theory Division, CH-1211 Geneva 23, Switzerland
(Dated: June 16, 2003)

We explore the consequences of a freeze-out criterion for heavy-ion collisions, based on pion escape probabilities from the hot and dense but rapidly expanding collision region. The influence of the expansion and the scattering rate on the escape probability is studied. The temperature dependence of this scattering rate favors a low freeze-out temperature of ∼100 MeV. In general, our results support freeze-out along finite four-volumes rather than sharp three-dimensional hypersurfaces, with high-$p_\perp$ particles decoupling earlier from smaller volumes. We compare our approach to the proposed universal freeze-out criteria using the pion phase-space density and its mean free path.

arXiv:nucl-th/0207074v3 16 Sep 2003

I. INTRODUCTION

Experiments with nuclear collisions at ultrarelativistic energies are performed with the aim of studying strongly interacting matter under high temperature and density. Such conditions are created very early in the collision. Hadrons at low transverse momentum form the bulk of the particles produced in these collisions. They are produced at the end of the hot and dense partonic phase, but they subsequently scatter in the confined hadronic phase prior to decoupling from the collision system ("freeze-out"). In general, the collective evolution of the hot and dense matter leaves a distinct imprint on the phase space distribution of the fireball at freeze-out. For example, pressure gradients generated in the early stage of the collision and indicative of the equation of state result in collective transverse, radial and elliptic flow which shape important features of hadronic one- and two-particle spectra. However, to disentangle such information from features generated during freeze-out a refined understanding of the decoupling process is needed. This is the condition which has to be satisfied locally for decoupling to take place.

Freeze-out is often modeled as a sudden breakup of the fireball on a fixed three-dimensional hypersurface [2], specified e.g. by a critical freeze-out temperature or density. This implements in a very simplified way the physical picture that the hadronic scattering rate drops with particle phase space density and determines freeze-out. However, the current difficulties in interpreting the HBT spectra measured at RHIC [1] motivate to go beyond a sharp three-dimensional implementation of freeze-out. Moreover, the recently observed increase in average pion phase space density from SPS ($\sqrt{s} = 17\,A$GeV) to RHIC ($\sqrt{s} = 130\,A$GeV) [9, 10] indicates that—in contrast to an earlier suggestion [8]—additional factors beyond the particle phase space density must be taken into account. This prompts us in the present work to discuss quantitatively how hadrochemical composition [6, 7], local temperature and collective velocity gradients [5], and particle momentum influence the decoupling of particles from the collision region. Since hadrochemistry does, and freeze-out temperature or velocity gradients may change in going from SPS to RHIC energies, this study also addresses the possible dependence of hadronic freeze-out on bombarding energy.

Clearly, in the general case, particles decouple from the fireball gradually [3, 4], as it is naturally implemented e.g. in cascade generator simulations. The question arises to what extent this generic behavior can be described by the limiting case of a sharp three-dimensional freeze-out. To discuss this question, we first introduce in Section II the so-called escape probability which characterizes the probability of a particle to decouple from the system. In Section III we demonstrate on simple examples how the escape probability is related to the expansion strength and the scattering rate. This illustrates the old suggestion [5], that freeze-out happens when the dilution rate becomes comparable or larger than the scattering rate. Moreover, the scattering rate depends on densities of individual species and the corresponding cross-sections [6, 7]. For pions, e.g., scattering on nucleons is much more important than scattering on other pions due to the larger cross-section of the former. In Section IV, we discuss the impact of the hadrochemical composition on the scattering rates and freeze-out at SPS and RHIC. This also allows to address the observed change in freeze-out phase space density [9, 10]. Finally, we turn to the dependence of the scattering rate and escape probability on temperature. In doing so, we find that $\approx 50\%$ of the particles are emitted at temperatures below ~ 100 MeV. We discuss this result, together with other findings of our calculations in Section V.

II. THE ESCAPE PROBABILITY

The following discussion of the freeze-out process [3, 4] is based on the particle escape probability $\mathcal{P}(x,p,\tau)$ defined as

$$f_{\rm esc}(x,p,\tau) = \mathcal{P}(x,p,\tau) f(x,p,\tau)\,. \qquad (1)$$

Here, $f(x,p,\tau)$ is the distribution function of a given particle species and $f_{\rm esc}(x,p,\tau)$ denotes the distribution of that fraction of particles which have decoupled from the system prior to time τ and will not rescatter in the fu-

ture. For a particle with momentum p at space-time point (x,τ), the probability to escape the medium without future interaction is [3, 4]

$$\mathcal{P}(x,p,\tau) = \exp\left(-\int_\tau^\infty d\bar\tau\, \mathcal{R}(x+v\bar\tau,p)\right). \quad (2)$$

Here, the scattering rate $\mathcal{R}(x,p)$ denotes the inverse of the mean time between collisions for a particle at position x with momentum p. The *opacity integral* in (2) determines the average number of collisions of the particle after time τ. Thus, for a particle which tries to escape the medium at time τ with velocity v, eq. (2) determines the probability that the particle succeeds to do so.

The limiting case of a sharp freeze-out along the three-dimensional proper time hypersurface given by $\tau_{\rm fr}$ [2] can be characterized by an abrupt change of the particle escape probability (2) from zero to one

$$\mathcal{P}(x,p,\tau)^{3-\rm dim.}_{\rm freeze-out} = \begin{cases} 0 & \text{for} \quad \tau < \tau_{\rm fr}\,, \\ 1 & \text{for} \quad \tau > \tau_{\rm fr}\,. \end{cases} \quad (3)$$

Freeze-out along more general three-dimensional hypersurfaces [2] can be defined by requiring this kind of threshold behavior of the escape probability along those hypersurfaces. It corresponds to a scattering rate which changes abruptly from a large value to zero along the freeze-out hypersurface.

Hypersurfaces of the type (3) are characterized by a criterion which tests *only the medium*, but does not depend on the particle momentum and particle properties. In the general case of continuous freeze-out, the situation is different since freeze-out does depend on particle momentum and properties. To characterize the four-volume from which particles decouple, one requires [4]

$$p^\mu \partial_\mu \mathcal{P}(x,p,\tau) > 0\,. \quad (4)$$

This specifies the region in which the amount of escaped particles of momentum p^μ is growing. Note that this general condition also characterizes the freeze-out hypersurface in case of the sharp freeze-out according to eq. (3). Condition (4) assumes, however, that there is no additional particle production, i.e., $p^\mu\partial_\mu f(x,p,\tau) = 0$. In the presence of such particle production, one generalizes (4) to $\partial_\mu(p^\mu \mathcal{P} f) > 0$.

In general, the evaluation of the criterion (4) is complicated. In the Discussion, we shall consider a related, much simpler condition which gives some access to the structure of a four-dimensional freeze-out region on the basis of the escape probability.

III. THE DEPENDENCE OF PARTICLE FREEZE-OUT ON EXPANSION

It has been argued a long time ago [5] that freeze-out happens when the dilution rate becomes larger than the collision rate. Here, we demonstrate how the collision rate and the expansion strength determine the escape probability.

To this end, we consider the simplified case of a particle of vanishing transverse momentum in the center of the fireball. Such a particle does not propagate through layers of different density but—due to expansion—finds itself in a medium of decreasing density. This simplification allows to illustrate the effect of dynamical properties of the collision region on freeze-out without being sensitive to further complications of the general case such as finite-size effects which depend on the production point and velocity of the test particle. We start the discussion of the escape probability (2) by considering a simple power-law ansatz for the scattering rate

$$\mathcal{R}(p=0,\, r=0,\, \tau) = \mathcal{R}(\tau) = \mathcal{R}_0 \left(\frac{\tau_0}{\tau}\right)^\alpha, \quad \alpha > 1\,, \quad (5)$$

Here, $\mathcal{R}_0$ is the scattering rate at the time τ_0. Below, we detail soon the assumptions on which (5) is based and how the exponent α characterizes the expansion strength of the system. To set the stage, however, we consider first the opacity integral of (5),

$$\int_{\tau_0}^\infty d\tau\, \mathcal{R}(\tau) = \frac{\mathcal{R}_0\tau_0}{\alpha-1}\,. \quad (6)$$

This illustrates the typical interplay of scattering and expansion: a given escape probability can be obtained for different values of the scattering rate, with a higher scattering rate $\mathcal{R}_0$ compensated by a stronger expansion (larger α).

We further illustrate this point with two analytically accessible models for the fireball expansion. Both are based on a factorized ansatz for the scattering rate in terms of the (averaged) cross-section σ for scattering in the medium, and the average velocity $\bar v_{\rm rel}$ relative to other particles,

$$\mathcal{R}(\tau) = \sigma\rho(\tau)\bar v_{\rm rel}\,. \quad (7)$$

While the time dependence of $\mathcal{R}$ does not factorize in the general case, one may hope to capture the dominant features of a realistic dynamical evolution by retaining the time dependence of the density, only.

For the first model, we choose a power-law fall-off of the density

$$\rho(\tau) = \rho_0 \left(\frac{\tau_0}{\tau}\right)^\alpha, \quad (8)$$

where ρ_0 is the density at the time τ_0. From this, the expression (5) can be recovered. This time-dependence of the density may not be realised during the whole evolution of the fireball; we assume it just in the final stage of the collision. Therefore, the time τ is now *defined* by the dilution rate γ

$$\gamma \equiv -\frac{1}{\rho}\frac{\partial\rho}{\partial\tau} = \frac{\alpha}{\tau}\,. \quad (9)$$

Even though we are interested in the situation along the longitudinal symmetry axis of the fireball, the time τ agrees with the "usual" longitudinal proper time $\sqrt{t^2-z^2}$ only if the density evolves according to (8) from the very beginning of the collision ($t=0$). Otherwise it corresponds to a different starting point t_0 of the time scale [31]

$$\tau = \sqrt{(t-t_0)^2 - z^2}\,. \tag{10}$$

This is analogous to the Hubble time in cosmology which is defined as the inverse of the expansion velocity gradient. We insert this dynamical information in the usual parametrization of the expansion four-velocity

$$\begin{aligned} u^\mu &= (\cosh\eta\,\cosh\eta_t(\tau,r)\,,\,\cos\phi\,\sinh\eta_t(\tau,r)\,, \\ &\quad \sin\phi\,\sinh\eta_t(\tau,r)\,,\,\sinh\eta\,\cosh\eta_t(\tau,r))\,. \end{aligned} \tag{11}$$

In accord with relation (10), the space-time rapidity is defined as

$$\eta = \frac{1}{2}\ln\left[\frac{(t-t_0)+z}{(t-t_0)-z}\right]\,,$$

and r, ϕ are the standard radial coordinates used in the plane transverse to the beam. The transverse rapidity η_t will be assumed to grow *linearly* with the radial coordinate. If the particle number is conserved, which is a good assumption at the end of the hadronic phase, the dilution rate is related to the divergence of the velocity field [12]

$$-\frac{1}{\rho}\frac{\partial\rho}{\partial\tau} = -\frac{1}{\rho}\,u^\mu\partial_\mu\rho = \partial_\mu u^\mu\,. \tag{12}$$

If we assume that $\eta_t(\tau,r) \propto r$, then eq. (12) links the four-velocity field (11) with the ansatz (8). This specifies the time dependence of the transverse rapidity

$$\eta_t(\tau,r) = \chi\frac{r}{\tau}\,, \tag{13a}$$

$$\chi = \frac{\alpha-1}{2}\,. \tag{13b}$$

In the vicinity of $r=0$, the choice $\chi=1$ leads to quasi-inertial flow which corresponds to an asymptotic solution of the fireball hydrodynamics [13]. The values $\chi<1$ and $\chi>1$ stand for radially decelerating and accelerating flow profiles, respectively. This illustrates the phenomenological consequences of a specific choice of the exponent α. Relation (13b) allows to rewrite the opacity integral (6)

$$\int_{\tau_0}^\infty d\tau\,\mathcal{R}(\tau) = \frac{\mathcal{R}_0\tau_0}{\alpha-1} = \frac{\mathcal{R}_0}{2}\left(\frac{\chi}{\tau_0}\right)^{-1}\,. \tag{14}$$

According to (13a), χ/τ_0 is the gradient of transverse rapidity at the time τ_0. At $r=0$, it is to a good approximation equal to the transverse velocity gradient. This substantiates the statement made above: a higher scattering rate can be compensated by a stronger transverse flow and still lead to the same escape probability. We note that it is not the average flow velocity, but the local flow *gradient* which determines the local density decrease and thus enters (14). In Appendix A we relate this result to the freeze-out criterion requiring the scattering rate to be smaller than the dilution rate [5].

For a second simple dynamical model of the fireball evolution, we turn to recent hydrodynamic simulations [14]. These indicate that the transverse expansion at the freeze-out stage may be better described by the ansatz

$$\eta_t(\tau,r) = \xi r\,, \tag{15a}$$

$$\xi(\tau) = \text{const}\,, \tag{15b}$$

rather than by the expressions (8) and (13) used above. In this case, the variable τ is still given by the relation (10), but corresponds now to the inverse longitudinal gradient of the expansion velocity

$$\tau = (\partial_0 u^0 + \partial_3 u^3)^{-1}\,.$$

The ansatz (15) implies a different time-dependence of the density. From eq. (12), one finds for the density at the center of the fireball

$$\rho(\tau) = \rho_0\frac{\tau_0}{\tau}\,\exp\left(-2\xi(\tau-\tau_0)\right)\,, \tag{16}$$

where ρ_0 is again the density at the time τ_0. The corresponding opacity integral reads

$$\int_{\tau_0}^\infty d\tau\,\mathcal{R}(\tau) = \mathcal{R}_0\,\tau_0\,\exp(2\xi\tau_0)\,\Gamma(0,2\xi\tau_0)\,, \tag{17}$$

where $\Gamma(a,x)$ is the incomplete Γ-function [15]

$$\begin{aligned} \Gamma(a,x) &= \int_x^\infty dt\,t^{a-1}\,e^{-t}\,, \\ &= \Gamma(a) - \int_0^x dt\,t^{a-1}\,e^{-t}\,. \end{aligned}$$

Relation (17) is less transparent than (14) but it shows the same qualitative feature: stronger scattering can be compensated by transverse expansion and lead to the same escape probability.

IV. THE SCATTERING RATE IN A THERMAL MODEL

In the previous section, we studied the effect of expansion on freeze-out. We derived expressions for the opacity integral which depend on the scattering rate at a fixed time τ_0. Here we calculate this scattering rate and we study how it depends on hadrochemistry and temperature. In particular, we determine the scattering rate corresponding to the hadronic final states at SPS and RHIC.

The scattering rate for a test pion of momentum p due to interactions with particles of type i and momentum k can be written as [16, 17]

$$\frac{d\mathcal{R}_i(x,p)}{d^3k} = \rho_i(x,k)\,\sigma_i(s)\,\frac{\sqrt{(s-s_a)(s-s_b)}}{2\sqrt{m_\pi^2+p^2}\sqrt{m_i^2+k^2}}\,. \quad (18)$$

Here, $\sigma_i(s)$ denotes the total cross-section for collinear collision,

$$s_a = (m_i+m_\pi)^2\,, \quad (19)$$
$$s_b = (m_i-m_\pi)^2\,, \quad (20)$$

and the cms energy $s = s(k,p)$.

We assume that the distribution of scattering partners $\rho_i(x,k)$ is given by the equilibrium form. In this way we neglect the modification of the distribution function due to decoupling of some particles. Such approximation was argued to cause only a small error on the escape probability in the practically relevant cases [4]. Thus we write

$$\rho_i(x,k) = \frac{g_i}{(2\pi)^3}\,\left[\exp\left((E_k-\mu_i)/T\right)\pm 1\right]^{-1}\,, \quad (21)$$

where g_i is the degeneracy of the species, T is the temperature, $E_k = \sqrt{k^2+m_i^2}$ and the chemical potential μ_i fixes the total density. This is known to provide a good description of the hadronic final state at SPS and RHIC [18, 19].

The total scattering rate is obtained by integrating the expression (18) over momentum k and summing over all species i

$$\mathcal{R}(x,p) = \sum_i \int\, d^3k\,\frac{d\mathcal{R}_i(x,p)}{d^3k}\,. \quad (22)$$

All pion scattering rates are computed in the rest frame of the hadron gas. We include pions, (anti)nucleons, kaons, rhos, and (anti)deltas as scattering partners. The total cross section of pion-baryon scatterings is parameterized as [20]

$$\sigma(\sqrt{s}) = \sum_r \frac{\langle j_i,\, m_i,\, j_\pi,\, m_\pi \,||\, J_r,\, M_r\rangle\,(2S_r+1)}{(2S_i+1)(2S_\pi+1)} \times\frac{\pi}{p_{\rm cms}^2}\,\frac{\Gamma_{r\to\pi i}\Gamma_{\rm tot}}{(M_r-\sqrt{s})^2+\Gamma_{\rm tot}^2/4}\,. \quad (23)$$

This is the usual Breit–Wigner resonance formula where M_r is the resonance mass and $\Gamma_{\rm tot}$ and $\Gamma_{r\to\pi i}$ are the total and the partial width for the given decay channel, respectively. Summation in (23) runs over all relevant resonance states listed in [20]. Momentum in the cms is denoted as $p_{\rm cms}$. The pre-factor takes care of proper counting of spin and isospin states. The square of Clebsch–Gordan coefficient $\langle j_i,\, m_i,\, j_\pi,\, m_\pi \,||\, J_r,\, M_r\rangle$ assures that the appropriate fraction of the resonance state is picked in coupling of the isospin states of the two scattering partners. Particle properties are taken from [21] except for higher excitations with large uncertainties which are taken from [20]. For scattering on both strange and non-strange mesons, the formula (23) is used again and a 5 mb momentum-independent contribution is added to account for elastic processes. The cross-section with baryons is taken to saturate at 30 mb for $\sqrt{s}$ above 3 GeV/c. This, however, has a negligible effect on the calculation since high momentum particles are suppressed in the thermal distribution.

To fix the hadrochemical composition of scattering partners at SPS and RHIC, an estimate of the chemical potentials entering (21) is needed. We take the chemical potential for direct pions from data on pion phase-space densities, and those for all other particle species from ratios of dN/dy at midrapidity. For SPS at $\sqrt{s} = 17\,A$GeV and RHIC at $\sqrt{s} = 130\,A$GeV we determine the chemical potentials for three different temperatures: 90, 100 and 120 MeV.

In more detail: the pion chemical potential at the SPS is obtained by comparing the $m_\perp$-dependence of the average phase-space density measured by NA44 [22] and WA98 [23] to the result expected from a thermalized boost-invariant source with box transverse density profile and a transverse flow profile $\eta_t = \sqrt{2}\eta_f r/R_{\rm box}$ [24]. The transverse momentum spectra relate transverse flow and temperature, such that $\eta_f \simeq 0.7$ corresponds to $T =$ 90 – 100 MeV and $\eta_f \simeq 0.55$ for $T = 120$ MeV. From the ratios of dN/dy at mid-rapidity measured for pions, protons, antiprotons, positive and negative kaons [25, 26], particle densities and corresponding chemical potentials are extracted under the assumption that all particles originate from the same thermal source, in accord with the use of equilibrated distribution in eq. (18). Resonance decay contribution to pion production is accounted for. The density of neutrons is assumed to be the same as that of protons. Chemical potentials for ρ's, Δ's and $\bar{\Delta}$'s are deduced by requiring detailed balance [27]

$$\mu_\rho = 2\mu_\pi\,, \quad \mu_\Delta = \mu_p+\mu_\pi\,, \quad \mu_{\bar\Delta} = \mu_{\bar p}+\mu_\pi\,. \quad (24)$$

The chemical potentials extracted in this way are summarized in Table I. The upper and lower values of μ's were chosen such that our parameters over- or underpredict the data by at least the maximal amount allowed by the quoted error bars. This ensures insensitivity of our conclusions against fine-tuning of parameters.

The same procedure is repeated for RHIC at $\sqrt{s} =$ 130 AGeV. Results are summarized in Table II. The yields at mid-rapidity for pions, (anti)protons, and kaons were taken from [28]. Unlike at SPS, the feed-down to (anti)proton yields from weak decays was not corrected for in the used data. We performed a simple correction by assuming that the yields of Λ's and Σ's are given by the same temperature and their chemical potentials equal to that of the protons. The preliminary data on pion phase-space density presented recently by STAR show small statistical error bars only [9], and lie close to the upper bound of the large systematic errors quoted earlier [10].

temperature	90 MeV	100 MeV	120 MeV
μ_p	477 – 497	435 – 455	350 – 379
$\mu_{\bar{p}}$	301 – 321	238 – 259	114 – 143
μ_π	50 – 65	38 – 53	10 – 30
μ_Δ	527 – 562	473 – 508	360 – 409
$\mu_{\bar{\Delta}}$	351 – 386	276 – 312	124 – 173
μ_ρ	100 – 130	76 – 106	20 – 60
μ_K	162 – 182	132 – 153	72 – 102
$\mu_{\bar{K}}$	111 – 131	76 – 96	4 – 33

TABLE I: Chemical potentials in units of MeV used in the calculation for SPS at $\sqrt{s} = 17\,A$GeV.

temperature	90 MeV	100 MeV	120 MeV
μ_p	442 – 489	393 – 452	291 – 373
$\mu_{\bar{p}}$	407 – 458	354 – 418	245 – 332
μ_π	78 – 100	70 – 97	50 – 85
μ_Δ	520 – 589	463 – 549	341 – 458
$\mu_{\bar{\Delta}}$	485 – 558	424 – 515	295 – 417
μ_ρ	156 – 200	140 – 194	100 – 170
μ_K	194 – 242	170 – 229	120 – 202
$\mu_{\bar{K}}$	179 – 230	153 – 217	100 – 187

TABLE II: Chemical potentials in units of MeV used in the calculation for RHIC at $\sqrt{s} = 130\,A$GeV.

Our analysis accounts for this not fully clarified experimental situation by associating to the central value of the most recent data [9] the large (asymmetric) systematic errors of [10]. To avoid a bias in relating SPS and RHIC energies, we compare the upper bound of the chemical potential for RHIC in Table II (which corresponds to the central value in [9]) to the upper bound listed in Table I for SPS. We thus underestimate the difference between RHIC and SPS.

Figure 1 shows the corresponding scattering rates for $T = 100$ MeV. The smaller contribution of nucleons at RHIC is largely compensated by antinucleons. Despite the increased pion phase-space density at RHIC, the pionic contribution does not dominate the total scattering rate because of the small pion-pion cross section. Scattering on pions is of comparable importance to scattering on nucleons and antinucleons: both particle species lead to a momentum averaged scattering rate of $\sim 0.2\,(\mathrm{fm}/c)^{-1}$.

We observe that the increase of pion phase-space density at RHIC when compared to SPS [9, 10] has no significant impact on the scattering rate. The earlier suggestion that the pion phase-space density at the freeze-out should be a universal quantity [8] did not account for the contribution of other particle species to the pion scattering rate.

Figure 2 summarizes our results for the various sets of freeze-out temperature and chemical potentials which limit the range of values consistent with data from SPS and RHIC. Although particle densities are approximately the same for all temperatures, the scattering rate increases significantly with temperature. On the other hand we see a generic decrease of the scattering rate with the pion momentum. This behavior is mainly dictated by phase-space available for the collisions, but also depends on the cross-section as a function of s. We discuss this behavior in more detail in Appendix B.

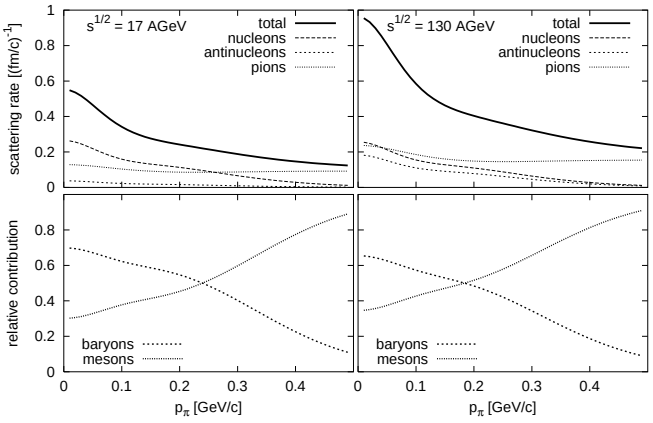

FIG. 1: Pion scattering rate as a function of pion momentum at $T = 100\,$MeV and the highest possible values of chemical potentials for SPS (left column) and RHIC (right column). Contributions to the total scattering rate from scattering on nucleons, antinucleons and pions are indicated. The lower row shows the baryonic and mesonic relative contributions.

In the lowest panel of Fig 2 we compare the extreme results for SPS and RHIC. If the scattering rate in one of the systems was clearly larger than in the other one, this would indicate a stronger transverse expansion in that system, as follows from Section III. We see that the present data do not allow to make any conclusion on this subject just by using the scattering rate.

V. CONCLUSIONS

In this paper, we have have calculated the scattering rates of pions which are characteristic for the late hadronic phase of the collisions at SPS and RHIC. We also illustrated for simple examples how these scattering rates determine the escape probability, and how the escape probability is affected by velocity gradients. Moreover, we found that the temperature dependence of the scattering rate allows to constrain the range of temperatures at which pion emission is significant. To estimate this temperature range, we combined the scattering rates of Section IV with the expressions for the opacity integral (14) and (17). Here, we discuss what is needed to overcome the limitation of our approach and what our results imply for freeze-out in the realistic case.

To go beyond the calculations presented here will require a refined dynamical model which follows the full space-time evolution of the fireball. Most likely, this will

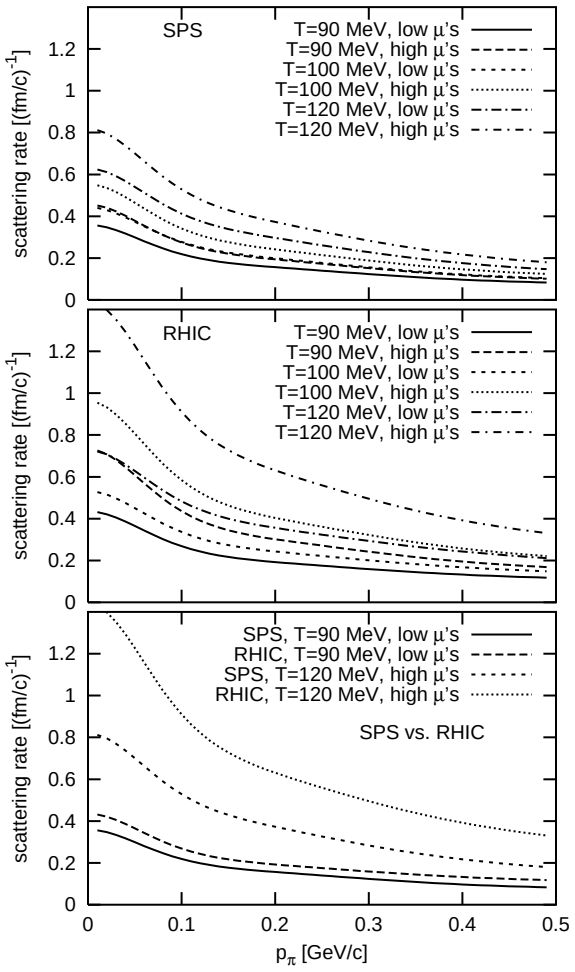

FIG. 2: Pion scattering rate as a function of pion momentum calculated for temperatures 90, 100, and 120 MeV and all corresponding sets of chemical potentials from Tables I (SPS at $\sqrt{s} = 17\ A$GeV) and II (RHIC at $\sqrt{s} = 130\ A$GeV). Lowest panel summarizes the lowest and the highest curves from both SPS and RHIC.

involve numerical simulations. In particular, one may hope to extend in this way the expressions for the opacity integral in Section III to the case of particles with finite momentum. For a realistic scenario, we envisage the following additional effects:

(i) In a transversely expanding fireball, particles with $p_\perp > 0$ are produced from parts of the system that co-move transversely. Their momentum relative to the medium p_π is thus smaller than $p_\perp$. The corresponding scattering rate $\mathcal{R}(p_\pi)$ is thus higher than the naively expected value at $p_\perp$. Hence, this effect *lowers* the escape probability.

(ii) A particle with finite $p_\perp$ can escape the fireball region in a finite time. Thus, the corresponding opacity integral (2) receives a contribution from a finite time only, in contrast to the infinite time which is accumulated by a test particle with $p_\perp = 0$ in our simplified calculation. This effect leads to a lower value of the opacity integral and *enhances* the escape probability.

Also, the evaluation of the general freeze-out criterion (4) is complicated and requires a complete knowledge of the space-time evolution of the fireball. To gain some understanding of the freeze-out process from the models studied here, however, it is instructive to turn to a simpler condition. Let us define freeze-out for particles at position x with momentum p to occur if the corresponding escape probability $\mathcal{P}(x,p)$ increases above a certain threshold value. Doing this, we actually specify a three-dimensional hypersurface on which a given fraction $f_{\rm esc}/f = \mathcal{P}$ of all particles is already decoupled. However, in contrast to previous freeze-out criteria [7, 8, 11], this condition does not only depend on the medium, but also on the particle momentum. Moreover, we can access some properties of the whole four-dimensional freeze-out region by varying the threshold value for $\mathcal{P}$. In this way, the above model calculations give some insight into freeze-out criteria which are more general than the Cooper-Frye type. To put in numbers: A realistic estimate of the transverse flow gradient $\xi = 0.08\,\mathrm{fm}^{-1}$ and the Bjorken freeze-out time $\tau_0 = 10\,\mathrm{fm}/c$ is taken from [18]. The value $\xi = 0.08\,\mathrm{fm}^{-1}$ is also in agreement with hydrodynamic simulations [14]. In order to achieve the escape probability of at least 1/3, the opacity integral must be smaller than $-\ln 1/3 \approx 1.1$. Then, eq. (14) leads to a scattering rate of less than $0.18\,(\mathrm{fm}/c)^{-1}$ while eq. (17) puts the upper limit for the scattering rate to $0.26\,(\mathrm{fm}/c)^{-1}$. At a temperature of 120 MeV, such a low value of the scattering rate is possibly reached at RHIC for $p_\pi > 0.4\,\mathrm{GeV}/c$ and at SPS at $p_\pi > 0.3\,\mathrm{GeV}/c$, as seen in Fig. 2. If we increase the required escape probability to 1/2, the scattering rate must be smaller 0.11 or 0.16, according to eqs. (14) and (17), respectively. For particles with $p_\pi < 0.4\,\mathrm{GeV}/c$, the temperature has to drop to 100 MeV if $\mathcal{P}$ should reach 1/2. Particles with $p_\pi < 0.2\,\mathrm{GeV}/c$ must wait even longer. On the other hand, if we put the required value of $\mathcal{P}$ to 0.1, eq. (17) leads to an upper bound of $0.54\,(\mathrm{fm}/c)^{-1}$ for the scattering rate. In the case of $T = 120\,\mathrm{MeV}$ and high μ's at RHIC pions with $p_\pi > 0.25\,\mathrm{GeV}/c$ fulfill this condition; in the less extreme cases, the 10% escape probability is reached by almost all pions.

This illustrates that particles decouple from the fireball gradually. It indicates that $\approx 10\%$ of the pions are decoupled at $T = 120\,\mathrm{MeV}$, but approximately half of them will escape at local temperatures below 100 MeV. Thus, a large fraction of the particles decouples at rather low temperatures. We note that a temperature of 120 MeV was assumed as a freeze-out temperature in a recent work [7] where a pion mean free path $\approx 1\,\mathrm{fm}$ was suggested as the universal freeze-out criterion. This work neglects the temperature dependence of the escape probability and its dependence on the momentum of the particle. Also,

it does not consider the possible cancellation between stronger scattering and stronger transverse expansion. In our approach, a thermal distribution of $T = 120\,\mathrm{MeV}$ at RHIC results in a pion mean free path of only 1.7 fm, only slightly larger than [7]. However, only 10 % of all particles are decoupled at this temperature. At lower temperatures, where the fraction of decoupled particles reaches 50%, we find a significantly larger average pion mean free path of at least 3–5 fm.

Let us further comment on the significance of the momentum dependence of the scattering rate. As discussed earlier, at certain $p_\perp$ the particle has a momentum with respect to the surrounding medium $p_\pi < p_\perp$, and thus the $p_\perp$-dependence of the scattering rate can be flatter than what is plotted in Fig. 2. We expect, however, that the monotonic increase of the escape probability with $p_\perp$ will be robust against refinements of our calculation. This suggests that in contrast to the idealization of a sharp freeze-out along a three-dimensional hypersurface, particle escape is ordered in momentum with high-$p_\perp$ particles freezing-out earlier and thus originating from a smaller fireball. This effect could lead to a stronger transverse mass dependence of HBT radii [29] than what is found in current model studies based on a Cooper-Frye freeze-out condition. These latter models (see e.g. the *blast-wave model* discussed in [30]) have difficulties in reproducing the observed strong $M_\perp$-dependence of HBT radii at RHIC. In what concerns the mechanism proposed here, one may envisage compensating effects: for example, if the transverse flow gradient is stronger at later times, then this will reduce the homogeneity regions measured by HBT radii at later times. Such a scenario seems unlikely since it implies acceleration of the collective expansion at a time when particles slowly cease to interact. However, to substantiate this expectation, a model which fully implements the fireball dynamics is needed. In our opinion, this warrants further investigations. In particular, hydrodynamical simulations should be revisited, which are typically based on sharp 3-dimensional freeze-out and thus miss any contribution from freeze-out along finite four-volumes.

We thank J.G. Cramer, U. Heinz, J. Pišút, and K. Redlich for fruitful discussions.

APPENDIX A: INTERPLAY OF THE SCATTERING RATE AND THE DILUTION RATE

Here, we give further details on the relation between the dilution rate and the scattering rate. We start from the opacity integral (6) and we express the exponent α in terms of the dilution rate γ via eq. (9). This leads to

$$\int_{\tau_0}^{\infty} d\tau\, \mathcal{R}(\tau) = \frac{\mathcal{R}_0 \tau_0}{\alpha - 1} = \frac{\mathcal{R}_0}{\gamma - \frac{1}{\tau_0}}\,. \qquad \text{(A1)}$$

This can be directly compared to the statement [5] that freeze-out happens when the dilution rate is at least as big as the scattering rate. For the scenario of continuous freeze-out considered here, a reasonable escape probability is reached when the opacity integral is of order one or smaller. In the model of eqs. (5) and (7) this leads to the condition

$$\gamma - \frac{1}{\tau_0} \gtrsim \mathcal{R}_0\,,$$

i.e., there is a factor $-1/\tau_0$ in addition to the standard criterion $\gamma \gtrsim \mathcal{R}_0$ [5]. The details of the relation between the scattering rate and the dilution rate at the freeze-out will depend on the particular time evolution of $\mathcal{R}$ and ρ, but the feature that larger $\mathcal{R}$ can be compensated by larger γ is generic.

APPENDIX B: GENERAL EXPRESSION FOR THE SCATTERING RATE

In this appendix we derive a general expression for the scattering rate. This allows us to investigate its dependences on temperature and the test particle momentum.

Following eq. (22) we write the scattering for some particle species of mass m. Assuming a Boltzmann distribution of the scattering partners and suppressing the position dependence,

$$\mathcal{R}(p) = \int \frac{d^3k}{(2\pi)^3}\, g\, \exp\left(-\frac{E_k - \mu}{T}\right) \times \sigma(s)\, \frac{\sqrt{(s-s_a)(s-s_b)}}{2\sqrt{m_\pi^2 + p^2}\sqrt{m^2 + k^2}}\,. \qquad \text{(B1)}$$

If we change the integration variables to the center of mass energy s and the energy of the scattering partner E_k, and perform the E_k-integration, this integral leads to

$$\mathcal{R}(p) = \frac{g\, e^{\mu/T}}{8\pi^2\, p\sqrt{p^2 + m_\pi^2}} \times \int_{(m_\pi+m)^2}^{\infty} ds\, \sigma(s) \sqrt{(s - m_\pi^2 - m^2)^2 - 4m_\pi^2 m^2} \times \sinh\left(\frac{p}{2Tm_\pi^2}\sqrt{(s - m_\pi^2 - m^2)^2 - 4m_\pi^2 m^2}\right) \times \exp\left(-\frac{\sqrt{p^2 + m_\pi^2}}{2Tm_\pi^2}(s - m_\pi^2 - m^2)\right)\,. \qquad \text{(B2)}$$

This scattering rate can be expressed as a convolution of the cross-section with the *"distribution of two-particle approaches"* $\mathcal{D}(p,s)$

$$\mathcal{R}(p) = \int_{(m_\pi+m)^2}^{\infty} \mathcal{D}(p,s)\, \sigma(s)\, ds\,. \qquad \text{(B3)}$$

By comparing with (B2), we obtain

$$\mathcal{D}(p,s) = \frac{g\, e^{\mu/T}\sqrt{(s-m_\pi^2-m^2)^2-4m_\pi^2m^2}}{8\pi^2\, p\sqrt{p^2+m_\pi^2}} \times \sinh\left(\frac{p}{2Tm_\pi^2}\sqrt{(s-m_\pi^2-m^2)^2-4m_\pi^2m^2}\right) \times \exp\left(-\frac{\sqrt{p^2+m_\pi^2}}{2Tm_\pi^2}(s-m_\pi^2-m^2)\right) . \quad \text{(B4)}$$

In the arguments of the exponential functions of (B4), the momentum of the test particle and the temperature are inversely related. Thus if one ignores the $1/p\sqrt{p^2+m_\pi^2}$ pre-factor, increasing T has the same effect as decreasing p. This offers an explanation why $\mathcal{R}$ increases with raising the temperature but decreases when the momentum becomes larger. There is no collision dynamics going into the calculation of $\mathcal{D}$; it represents merely the phase-space populated with thermally distributed scattering partners.

However, the temperature and momentum dependence of the scattering rate is not given solely by the distribution of two-particle approaches, but also reflects details of the convolution of $\mathcal{D}(p,s)$ with the scattering cross section $\sigma(s)$. This can be seen e.g. by comparing our results with those obtained in [16]. In that paper, the authors used a simple prescription $\sigma(s) \propto \delta(s-M_r^2)$ which leads to a qualitatively different dependence of the scattering rate on the test particle momentum. We verified that this is a consequence of neglecting the width of the resonance. By only assuming the lowest resonance states in a given channel and narrowing the resonance shape, we were able to reproduce the results of [16] as a limiting case of our calculation.

[1] S. Pratt, Nucl. Phys. **A715**, 389c (2003).
[2] F. Cooper and G. Frye, Phys. Rev. D **10**, 186 (1974).
[3] F. Grassi, Y. Hama and T. Kodama, Z. Phys. C **73**, 153 (1996).
[4] Yu.M. Sinyukov, S.V. Akkelin and Y. Hama, Phys. Rev. Lett. **89**, 052301 (2002).
[5] J. Bondorf, S. Garpman and J. Zimányi, Nucl. Phys. **A296**, 320 (1978).
[6] S. Nagamiya, Phys. Rev. Lett. **49**, 1383 (1982).
[7] D. Adamová *et al.* [CERES Collaboration], Phys. Rev. Lett. **90**, 022301 (2003).
[8] D. Ferenc, U. Heinz, B. Tomášik, U.A. Wiedemann and J.G. Cramer, Phys. Lett. B **457**, 347 (1999).
[9] R.L. Ray for the STAR Colaboration, Nucl. Phys. **A715**, 45c (2003).
[10] J.G. Cramer, talk at *INT RHIC Winter Workshop 2002, Jan. 6, 2002, Seattle, WA, USA*; `http://mocha.phys.washington.edu/~int_talk/WorkShops/RHIC02/People/Cramer_J/`.
[11] T. Alber *et al.* [NA35 Collaboration], Z. Phys. C **66**, 77 (1995).
[12] E. Schnedermann and U. W. Heinz, Phys. Rev. C **47**, 1738 (1993).
[13] S.V. Akkelin, T. Csörgő, B. Lukács, Yu.M. Sinyukov and M. Weiner, Phys. Lett. B **505**, 64 (2001).
[14] P.F. Kolb, arXiv: nucl-th/0304036.
[15] M. Abramowitz and I.A. Stegun eds., *Handbook of Mathematical Functions, Dover, New York, 1972.*
[16] M. Prakash, M. Prakash, R. Venugopalan, and G. Welke, Phys. Rep. **227**, 321 (1993).
[17] J. Ftáčnik, P. Lichard, N. Pišútová and J. Pišút, Z. Phys. C **42**, 139 (1989).
[18] B. Tomášik, U. A. Wiedemann and U. W. Heinz, Heavy Ion Physics **17**, (2003).
[19] T. Csörgő and A. Ster, arXiv:nucl-th/0207016.
[20] S. A. Bass *et al.*, Prog. Part. Nucl. Phys. **41**, 225 (1998).
[21] D. E. Groom *et al.* [Particle Data Group Collaboration], Eur. Phys. J. C **15**, 1 (2000).
[22] M. Murray and B. Holzer, Phys. Rev. C **63** 054901 (2001).
[23] M.M. Aggarwal [WA98 Collaboration], Phys. Rev. C **67**, 014906 (2003).
[24] B. Tomášik and U. W. Heinz, Phys. Rev. C **65**, 031902 (2002).
[25] J. Bächler *et al.* [NA49 Collaboration], Nucl. Phys. A **661**, 45 (1999).
[26] S. V. Afanasiev *et al.* [The NA49 Collaboration], Phys. Rev. C **66**, 054902 (2002).
[27] H. Bebie, P. Gerber, J. L. Goity and H. Leutwyler, Nucl. Phys. B **378**, 95 (1992).
[28] K. Adcox *et al.* [PHENIX Collaboration], Phys. Rev. Lett. **88**, 242301 (2002).
[29] F. Grassi, Y. Hama, S. S. Padula and O. J. Socolowski, Phys. Rev. C **62**, 044904 (2000).
[30] B. Tomášik, arXiv: nucl-th/0304079.
[31] Technically, if we were solving for the whole fireball evolution, we would have to match the prescription (8) and its first time-derivative to the time-dependence of the density at earlier times. This is done by tuning ρ_0 *and* τ_0. Therefore, τ_0 has to be a free parameter, and is not necessarily equal to the longitudinal proper time measured from the moment of the first approach of the colliding nuclei.